Amorphization dynamics of Ge2Sb2Te5 films upon nano- and femtosecond laser pulse irradiation

J. Siegel, W. Gawelda, D. Puerto, C. Dorronsoro, J. Solis et al.

Citation: J. Appl. Phys. **103**, 023516 (2008); doi: 10.1063/1.2836788
View online: http://dx.doi.org/10.1063/1.2836788
View Table of Contents: http://jap.aip.org/resource/1/JAPIAU/v103/i2
Published by the American Institute of Physics.

Amorphization dynamics of $Ge_2Sb_2Te_5$ films upon nano- and femtosecond laser pulse irradiation

J. Siegel,[1,a)] W. Gawelda,[1] D. Puerto,[1] C. Dorronsoro,[1] J. Solis,[1] C. N. Afonso,[1] J. C. G. de Sande,[2] R. Bez,[3] A. Pirovano,[3] and C. Wiemer[4]
[1]*Instituto de Optica, CSIC, Serrano 121, E-28006 Madrid, Spain*
[2]*Ingeniería de Circuitos y Sistemas, EUITT, UPM, Ctra. de Valencia km 7.5, 28031 Madrid, Spain*
[3]*STMicroelectronics, via C. Olivetti 1, Agrate Brianza I-20041, Italy*
[4]*MDM Laboratory, CNR-INFM, via C. Olivetti 2, Agrate Brianza I-20041, Italy*

(Received 10 October 2007; accepted 5 December 2007; published online 28 January 2008)

Phase transformations of crystalline $Ge_2Sb_2Te_5$ films upon pulsed laser irradiation have been studied using *in situ* reflectivity measurements with temporal resolution. Two different configurations allowed point probing with nanosecond temporal resolution and imaging with subpicosecond temporal and micrometer spatial resolution. The role of the pulse duration and laser fluence on the dynamics of the phase change and the degree of amorphization is discussed. Several advantageous features of femtosecond compared to nanosecond laser-induced amorphization are identified. Moreover, a high-resolution study of the amorphization dynamics reveals the onset of amorphization at moderate fluences to occur within ~100 ps after arrival of the laser pulse. At high fluences, amorphization occurs after ~430 ps and the molten phase is characterized by an anomalously low reflectivity value, indicative of a state of extreme supercooling. © *2008 American Institute of Physics*. [DOI: 10.1063/1.2836788]

I. INTRODUCTION

The concept of phase change data storage was demonstrated by S. R. Ovshinsky 40 years ago.[1] It is based on the switching of chalcogenide films between the amorphous and crystalline phase, having very different optical and electrical properties, by means of controlled heating and cooling. In phase change *optical* recording, the heat is delivered to the film by means of a short laser pulse and the data is also read out optically, exploiting the fact that the crystalline and amorphous phases have different reflectivities. Having appeared already in 1990 as a commercial product, phase change optical disks (PCODs) have achieved maturity and impressive performance.[2] More recently, *electrically* addressed storage devices, also based on phase changes in chalcogenides, have been developed, which are compatible with complementary metal oxide semiconductor (CMOS) technology. These so-called phase change memories (PCMs) rely on different electrical resistances of crystalline and amorphous phases and prototype devices have already been demonstrated by several manufacturers. PCMs are one of the most promising candidates for next-generation nonvolatile memories, having the potential to surpass the performance of flash memories, including scalability.[3]

Present research in phase change data storage is focused on further improving device performance (PCOD and PCM) in terms of capacity, archival lifetime, data transfer rate, etc. While high capacities (50 GB) and long lifetimes (>20 years) have already been reached, at least for PCODs and in today's Blu-ray disks, the maximum achievable data transfer rate seems still far from satisfactory. One reason is the technical difficulty to fabricate compact laser sources able to generate pulses shorter than a few tens of nanoseconds for triggering phase transitions, thus imposing a limit to the data transfer rate achievable. However, with the arrival and ongoing miniaturization of femtosecond laser pulse systems, this limitation has been overcome at the laboratory stage and should soon be overcome in commercial devices. Another fundamental limit on the data transfer rate is the phase change response of the recording material. The material currently employed in PCOD and PCM devices is usually a thin film of the GeTe $-Sb_2Te_3$ pseudobinary system. Yamada *et al.* reported already in 1991 reversible phase changes in three stoichiometric compositions of this system, $Ge_1Sb_4Te_7$, $Ge_1Sb_2Te_4$, and $Ge_2Sb_2Te_5$, using pulse durations as short as 30 ns.[4] Materials and pulse durations used in this pioneering work remain the standard of today's technology. Since amorphization requires melting and rapid quenching, shorter or even ultrashort pulses are inherently suitable because they are able to generate much higher cooling rates than nanosecond laser pulses.[5] In contrast, the inverse transformation is clearly not favored by using ultrashort laser pulses due to the existence of a minimum time required for stable crystalline nuclei to form and grow.

By careful tailoring of heat flow conditions of the film-substrate system, reversible phase changes were achieved in the 1990s (Refs. 6 and 7) in Ge_xSb_y films using picosecond and femtosecond pulses. The full phase transformation times for picosecond pulse irradiation of $Ge_{0.07}Sb_{0.93}$ films were determined to be around 400 ps both for crystallization and amorphization.[8] These results achieved in the binary GeSb system show that ultrafast reversible phase transformation can be achieved in the GeTe$-Sb_2Te_3$ system, if appropriate system conditions can be found. A first step in this direction has been made recently in which a suitable film-substrate system was identified to allow for reversible phase changes

a)Electronic mail: j.siegel@io.cfmac.csic.es.

in $Ge_2Sb_2Te_5$ triggered by 30 ps laser pulses,[9] 3 orders of magnitude shorter than the limit found by Yamada *et al.*[4] Recent studies on the influence of doping[10] or vacancies[11] in the $GeTe-Sb_2Te_3$ system have shown an alternative route to modify and speed up crystallization. However, reversible phase switching with femtosecond laser pulses still remains a challenge in the GeTe–SbTe system. A full understanding of the dynamics of the phase change is required in order to overcome it.

The aim of this work is to study the amorphization dynamics in $Ge_2Sb_2Te_5$ films upon pulsed laser irradiation with nanosecond and femtosecond laser pulses. It is evaluated by studying reflectivity changes during transformation with temporal resolution in two modalities. The first one, based on detecting a probe beam with a fast photodiode, provides a temporal resolution of a few nanoseconds and covers a broad temporal window. The second modality, femtosecond pump-probe microscopy,[12,13] provides a temporal resolution better than 1 ps and zooms into the time window of a few nanoseconds, in which melting, quenching, and amorphization are most likely to occur. Previous subnanosecond resolution studies, using picosecond laser pulses, have already revealed important details of the phase transition, such as the existence of three distinct stages, namely, rapid melting, solidification, and slow relaxation,[14,15] as well as the dominant influence of the thermal conductivity of the substrate to either facilitate or prevent amorphization.[9] The present work aims for a much higher temporal resolution in order to truly resolve the phase transformation induced by femtosecond laser pulses and to compare its dynamics to that induced by nanosecond laser pulses. Moreover, the technique used (femtosecond pump-probe microscopy) is capable of providing micrometer spatial resolution and is thus able to follow the transformation dynamics simultaneously at different spatial positions of the irradiated region, which correspond to different local laser fluences.[12,13,16]

The paper is organized as follows. Experimental details and conditions are given in Sec. II. The results are described and discussed in Sec. III, which is divided into two parts: The first part (Sec. III A) contains a comparative study of the amorphization process induced by nanosecond and femtosecond laser pulses, whereas the second part (Sec. III B) focuses on the amorphization dynamics induced with femtosecond laser pulses. The main results are summarized and conclusions drawn in Sec. IV.

II. EXPERIMENTAL APPROACH, DATA ANALYSIS, AND MODELING

The sputter-deposited samples used in this study consisted of 46 nm thick, face-centered-cubic polycrystalline and amorphous $Ge_2Sb_2Te_5$ films on Si(001) wafers with a sandwiched 10 nm thick SiO_2 buffer layer. The structure and the thickness of the films were determined by means of x-ray diffraction and x-ray reflectivity measurements, using an x-ray tool equipped with both a scintillator and a position-sensitive detector, already described elsewhere.[17] Measurements of the optical properties of the films were performed using a Woollam spectroscopic ellipsometer, covering a range from 350 to 1700 nm and measuring at different angles of incidence (76°, 78°, 80°, 82°, and 84° in the crystalline film and 78°, 80°, and 82° in the amorphous film). The refractive index and absorption coefficient were obtained by fitting the experimental data to the Tauc–Lorentz model.[18] The obtained values are consistent with those reported by Lee *et al.*[18] and have been used to model the expected reflectivity change upon amorphization progressing in depth. The model takes into account the complete sample system ($Ge_2Sb_2Te_5$ film, SiO_2 buffer layer, Si substrate) with their corresponding optical constants and thicknesses. Moreover, it takes into consideration a full coherent superposition of Fresnel reflections at all interfaces for a given probe wavelength at normal incidence.[13] Laser irradiation was performed using a regeneratively amplified Ti:sapphire laser system operating at 800 nm central wavelength with a pulse duration that could be switched from 120 fs to 8 ns by blocking the femtosecond oscillator seed laser. The *s*-polarized amplified laser beam was focused onto the sample at an angle of incidence of 54° to an elliptical spot size of 100×59 μm for measurements with nanosecond resolution and to 173×100 μm for those with subpicosecond resolution ($1/e^2$-intensity diameters). In both cases, we select a single laser pulse from a 100 Hz pulse train by means of an electromechanical shutter to irradiate an unexposed region of the sample. The temporal evolution of the surface reflectivity was measured by recording the reflected signal of a second laser beam probing the transforming region at normal incidence. Two different configurations were used. In the first one, point probing real-time reflectivity measurements, the probe laser was a frequency-doubled, continuous-wave, single-frequency Nd:yttrium aluminum garnet (YAG) laser emitting at 532 nm, whose output was focused to a spot size of $\sim 5 \times 5$ μm at the center of the region irradiated by the pump laser. The specular reflection of the probe light was collected and focused onto a fast photodiode connected to a fast oscilloscope, providing a temporal resolution of a few nanoseconds. In the second configuration, femtosecond pump-probe microscopy, a fraction of the pump pulse was frequency doubled to 400 nm (λ_{probe}) and used as a low-intensity probe pulse to illuminate the sample at a user-defined temporal delay after the arrival of the pump pulse. The probe light reflected from the sample was sent through an ad-hoc designed microscope equipped with a 12 bit charge-coupled device (CCD) camera, using a microscope objective ($20\times$, numerical aperture=0.42) and a tube lens, with a 10 nm bandpass filter centered at λ_{probe} placed in the imaging path. This setup allows recording snapshots of the surface reflectivity at different delay times after the arrival of the pump pulse. The temporal delay between pump and probe pulse is achieved by means of a motorized optical delay line covering a maximum delay of 1 ns and a manual delay line to extend the delay up to 22 ns. The temporal resolution of the system was slightly reduced by dispersion in the optical components to an estimated value of ~ 500 fs. Further details on the setup can be found elsewhere.[13] White light illumination images of the samples after irradiation were recorded in reflection with the *in situ* microscope setup described above, as well as with a separate standard white light microscope.

Analysis of the real-time reflectivity data with nanosecond resolution was straightforward by simply dividing the reflectivity signal trace recorded during laser irradiation by the trace recorded before laser irradiation. In the case of femtosecond pump-probe microscopy data, signal normalization was done by dividing the image recorded at a given delay after the pump pulse by an image taken before laser exposure. This procedure allows for correction of the spatial inhomogeneity of the illumination beam. Despite this correction, the normalized images did show superimposed intensity patterns that varied randomly for different irradiations. A careful study revealed that these patterns were caused by small spatial fluctuations of the femtosecond laser beam, which are inevitable because of the finite pointing stability of the laser system. As a consequence, a randomly changing lateral shift was produced between the intensity patterns of the image recorded before and during laser irradiation. Conventional methods to extract intensity cross sections through the normalized images turned out to be of little use because of the so-produced residual modulation. Although averaging several cross sections of neighboring pixel rows improved the signal-to-noise ratio somewhat, the extracted horizontal profiles still suffered from noise. In addition, the regions of sharp intensity transitions were flattened as a consequence of averaging neighboring pixel rows of an image with an elliptical feature. In order to overcome these problems, we performed radial averaging. First, the image dimensions were scaled such that the elliptical spot became circular. Second, all pixels at a given radial distance were averaged, effectively averaging along a circle. This was done for all radial positions, yielding a radial profile that starts in the spot center ($r=0$). This method exploits the complete 2D information contained in each image, e.g., each image pixel point is assigned its corresponding radial distance and contributes to enhance the signal-to-noise ratio at a given radial distance. Thus, the signal-to-noise ratio is lowest in the very center, where only few pixels are averaged, and increases toward larger radii. Moreover, this method preserves sharp radial intensity transitions. We note that this method can only be applied to intensity distributions with expected circular or elliptical symmetry. The validity of the method in our case is justified by the Gaussian intensity distribution of the pump laser beam at the sample plane, which induces phase transformations with elliptical symmetry.

III. RESULTS AND DISCUSSION

A. Amorphization induced by nanosecond and femtosecond laser pulses: A comparison

Figure 1(a) shows the reflectivity evolution of a crystalline sample as a function of time upon irradiation with single nanosecond and femtosecond laser pulses, as measured with the point probing real-time reflectivity measurement setup. The observed reflectivity decrease appears to occur on a similar time scale for both pulse durations and the reflectivity finally reaches the same constant level. The final level is well below the initial one and corresponds to the amorphous phase, as confirmed experimentally by recovering the initial reflectivity level of the crystalline phase upon irradiation of

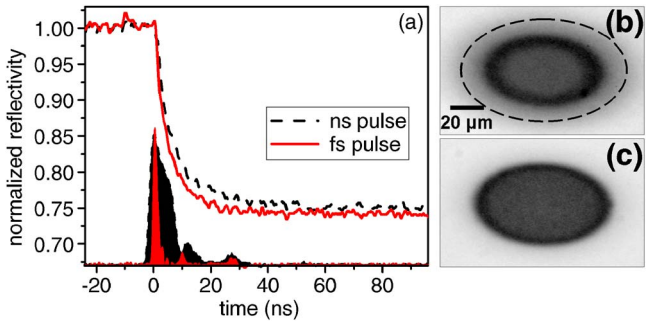

FIG. 1. (Color online) (a) Evolution of the reflectivity at 532 nm of a crystalline $Ge_2Sb_2Te_5$ film upon laser-induced amorphization using a single nanosecond laser pulse (154 mJ/cm^2, black dashed curve) and femtosecond laser pulse (66 mJ/cm^2, red solid curve). The corresponding laser pulse profiles are shown at the bottom (black=nanosecond pulse, red =femtosecond pulse). The reflectivity values are normalized to the reflectivity of the film before irradiation. The images were taken after irradiation with a nanosecond (b) and femtosecond (c) laser pulse, using white light microscopy. The dashed line in (b) marks the region of partial amorphization surrounding the amorphous spot in the case of nanosecond irradiation.

the amorphized region with a few laser pulses at low fluence (typically a third of the fluence value required for amorphization). Neither recrystallization of the amorphous spot nor crystallization of an amorphous sample could be achieved with a single laser pulse. The 90%–10% decay time extracted from the reflectivity data in Fig. 1(a) is ~20 ns upon nanosecond pulse irradiation and ~12 ns upon femtosecond pulse irradiation. It is well known that laser-induced amorphization requires melting as a previous step.[19] Assuming that solidification occurs interfacially toward the surface starting from the maximum melt depth, which is the most probable scenario, and considering the high thermal conductivity of the substrate and the thin buffer layer, the solidification velocities can be estimated by dividing the film thickness by the decay time. This estimation yields values of ~2.3 and ~3.8 m/s for the nanosecond and femtosecond pulse data, respectively. These velocities are relatively low compared to the critical amorphization velocities reported in elementary bulk semiconductors[20] but are comparable to those observed in thin films.[21] The femtosecond pulse-induced transformation is actually much faster, because the value estimated above is affected by the limited temporal resolution of the detection system.

The different nature of the phase transformation induced by nanosecond and femtosecond pulses can be appreciated in the white light microscope images in Figs. 1(b) and 1(c). For nanosecond laser pulses, a relatively large modified region with low optical contrast [outer gray ring in Fig. 1(b)] surrounds the amorphous spot. The transformation of this region is not caused by lateral heat flow from the central region. Under the present conditions of a spot size (100×59 μm) that is more than 3 orders of magnitude larger than the film thickness (46 nm), the dominant direction of heat flow is toward the substrate. The thermal diffusion length during the nanosecond pulse[9] is ~60 nm and thus much small than the spot size. This demonstrates that the modified outer ring in Fig. 1(b) is not caused by lateral heat flow but by the slow energy deposition at the wings of the Gaussian beam profile, causing a weak material modification (possibly partial amor-

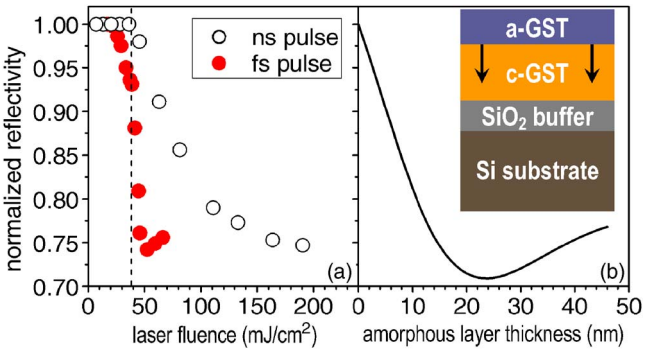

FIG. 2. (Color online) (a) Reflectivity level at 532 nm obtained several microseconds after irradiation with nanosecond and femtosecond laser pulses as a function of laser fluence, extracted from a series of reflectivity transients similar to those shown in Fig. 1. The dashed vertical line at about 38 mJ/cm^2 marks the change of slope of the femtosecond pulse data. (b) Calculation of the reflectivity change induced in the film upon transformation into the amorphous phase, starting from the surface. All reflectivity values are normalized to the reflectivity of the crystalline film at 532 nm before irradiation.

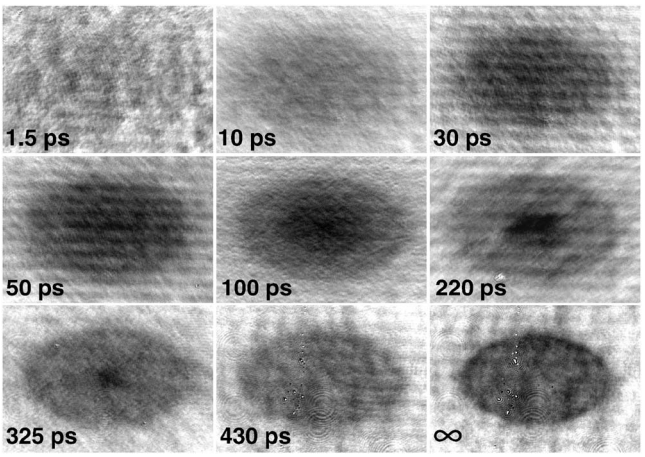

FIG. 3. Time-resolved surface reflectivity images (λ_{probe}=400 nm) of a crystalline $Ge_2Sb_2Te_5$ film at different delay times t (see image labels) after exposure to a femtosecond pump pulse. The peak fluence is 60 mJ/cm^2. The gray scale used is linear and the same for all frames. The frame size is 153×101 μm.

phization) as a consequence of partial melting and a reduced supercooling. The absence of this surrounding modified zone for femtosecond pulses in Fig. 1(c) is due to the instantaneous energy deposition possible with ultrashort pulses, generating conditions for strong supercooling that results in sharper transformation thresholds. While the ability of femtosecond pulses to achieve spots without a modified outer region has already been reported by Ohta *et al.*,[5] it was attributed to the absence of lateral heat flow. However, as the above estimation of the thermal diffusion length shows, lateral heat flow is not the issue for nanosecond pulses but the wings of the Gaussian beam profile in combination with heat flow to the substrate during the pulse.

The virtual absence of heat flow during the femtosecond laser pulse leads also to a more efficient energy deposition, which can be seen by the much lower fluence values (66 mJ/cm^2) required to achieve amorphization compared to nanosecond pulses (154 mJ/cm^2). This can also be appreciated in Fig. 2(a), showing the final reflectivity level obtained after irradiation as a function of the laser pulse fluence. The threshold for a measurable reflectivity decrease upon irradiation with single nanosecond pulses is ~40 mJ/cm^2, compared to ~20 mJ/cm^2 for femtosecond laser pulses. Moreover, the reflectivity drops much faster upon femtosecond than upon nanosecond irradiation, and two fluence regimes with different evolutions can be distinguished in the former case: a relatively slow decrease until ~38 mJ/cm^2 and an abrupt decrease at higher fluences.

The evolution of the reflectivity upon transformation from the crystalline film into a film with an amorphous surface layer, which increases in thickness as the laser fluence is increased, has been calculated using the model described in Sec. II. The result of the normalized reflectivity change is shown in Fig. 2(b). The calculated reflectivity evolution resembles the experimental data in Fig. 2(a), thus establishing a relationship between the quantities of the x axis of Figs. 2(a) and 2(b), i.e., the laser fluence and the thickness of the amorphized surface layer. This relationship implies the accomplishment of three conditions: First, the melt depth is a monotonous function of laser fluence. This condition is met whenever the laser fluence exceeds the threshold value for surface melting. Second, the supercooling generated in the molten layer by heat flow towards the substrate is sufficiently large, over the entire fluence range, to support nucleation and growth of the amorphous phase. This condition is met in our case because the heat extraction to the substrate is very efficient due to the large thermal conductivity of Si and the reduced thickness of the poorly conducting buffer layer. And third, the amount of latent heat released during solidification is small in order to maintain a sufficiently strong supercooling for amorphization to occur and suppress recalescence effects.[21] This condition is likely met because the amount of latent heat released is proportional to the thickness of the $Ge_2Sb_2Te_5$ film,[8] which in our case is small.

The maximum optical contrast (normalized reflectivity change) predicted by the calculation (~−29%) in Fig. 2(b) agrees well with the experimental data (~−26%) upon nanosecond and femtosecond pulse irradiation in Fig. 2(a). Moreover, the femtosecond pulse data shows an inflection point at 52 mJ/cm^2, which corresponds in the model to the minimum observed in the calculation for an amorphous surface layer of ~24 nm. The subsequent increase of the level for higher fluences is consistent with the calculation and indicates that the film has been amorphized throughout its whole thickness. In contrast, the absence of an inflexion point in the nanosecond pulse data indicates that less than 24 nm have been transformed into the amorphous phase. An increase in laser fluence beyond the data range shown in Fig. 2(a) leads to film ablation, the ablation threshold values being 210 and 70 mJ/cm^2 and for nanosecond and femtosecond pulses, respectively.

B. High-resolution study of the amorphization dynamics induced by femtosecond laser pulses

In the case of femtosecond pulse irradiation, we have performed a complementary study of the amorphization dynamics using femtosecond pump-probe microscopy. Figure 3

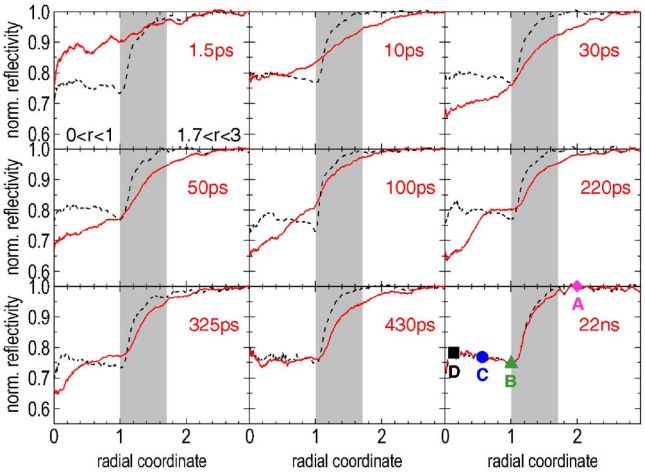

FIG. 4. (Color online) Radial profiles of the reflectivity extracted from the series of images shown in Fig. 3 following the procedure described in Sec. II. The reflectivity values are normalized to the reflectivity of the crystalline film at 400 nm before irradiation. The dashed black curves correspond to profiles recorded several seconds after irradiation ($t=\infty$) and the solid red curves to profiles recorded at delay t, indicated in the label of each frame. The radial coordinate has been normalized to the maximum extension of the region of (almost) complete amorphization. The shaded areas mark the regime of partial amorphization ($1<r<1.7$) sandwiched between the regime of amorphization of an optically thick layer ($0<r<1$) and that of heating without phase transformation ($1.7<r<3$). The plot at $t=22$ ns marks characteristic radial positions A, B, C, and D (and thus different local fluences) used for analysis and the representation in Fig. 5.

shows a series of images of the surface of the crystalline sample illuminated by the femtosecond probe pulse at different delays after the arrival of a femtosecond pump pulse with a peak fluence of 60 mJ/cm^2. The evolution of the optical changes shows a gradual homogeneous darkening of the irradiated area up to a delay of 50 ps, which corresponds to occurrence of film melting. For further-increasing delays (100–325 ps), the dark region shrinks gradually, leaving behind a ring with a reflectivity that is higher than that of the dark region but lower than the unexposed region. The dark region vanishes completely at $t=430$ ps, and the phase left behind resembles very much the final amorphous phase, as can be seen by comparison with the image recorded several seconds after the arrival of the pump pulse ($t=\infty$).

Radial reflectivity profiles (at 400 nm) of the normalized images recorded at different delays (Fig. 3) have been extracted according to the procedure described in Sec. II and are shown in Fig. 4. The radial coordinate r refers to the radial distance of the corresponding intensity value from the center of the spot, after having rescaled the elliptical intensity distribution to a circular one. Because of this rescaling, we keep the r coordinate in arbitrary units to avoid confusion between horizontal and vertical physical dimensions. Because the pump beam has a well-defined (Gaussian) spatial intensity distribution, different radial positions correspond to different local fluences. For each transient profile (red solid curves in Fig. 4) at a given delay, the corresponding final profile (black dashed curves in Fig. 4) obtained several seconds after irradiation ($t=\infty$) is also included. As explained in Sec. II, the small differences between the profiles at $t=\infty$ are due to the residual modulation in the normalized images and due to pulse-to-pulse fluctuations of the probe beam intensity ($\sim\pm 8\%$). The appearance of noise spikes at very low r-values (0–0.1) in the transient and final profiles is caused by the low number of pixels at this radial position.

The potential of the radial profile method becomes evident when looking at the transient profile obtained at $t=1.5$ ps, which shows a clear transient reflectivity decrease below 1 (reflectivity values normalized to the reflectivity before irradiation), something that cannot be appreciated from the corresponding nonprocessed image in Fig. 3. At increasing delays, the reflectivity decrease gets not only more pronounced but also extends beyond the region showing permanent optical changes ($t=\infty$ curve, $0<r<1.7$), reaching its maximum extension ($0<r<2.5$) at $t=30$ ps. The region $1.7<r<2.5$, exposed to much lower local fluences than the center, fully recovers the initial reflectivity value after irradiation ($t=\infty$), which indicates that the material in this region is only heated by the laser pulse but not structurally modified. The "transition region" ($1<r<1.7$, shaded in gray in Fig. 4) between this heated outer region and the fully amorphized region in the center corresponds to a region in which amorphization has only occurred in a thin surface layer. Also, here (as in the outer region) the reflectivity changes smoothly with time. Note that the relative spatial extension of this transition region is much smaller than in the case of nanosecond irradiation [cf. Figs. 1(b) and 1(c)].

Very different, however, is the temporal evolution in the central region ($0<r<1$), which eventually transforms into an optically thick amorphous phase. Here, the radial reflectivity distribution continuously decreases until a delay of 30–50 ps, when it changes strongly. At longer delays, the spatial extension of the minimum starts to shrink, consistent with the observations in Fig. 3, where the dark region, attributed to the liquid phase, disappears at $t=430$ ps, leaving behind an approximately constant reflectivity value up to $r=1$. The good match of the transient reflectivity profile at this delay with the final profile after irradiation area ($t=\infty$) within the central region ($0<r<1$) indicates that already at $t=430$ ps the entire region has been transformed from the crystalline into the amorphous phase. If we assume that the peak fluence in the spot center is sufficient to melt throughout the entire film, an estimation of the solidification velocity yields a value of ~ 100 m/s, much higher that the one estimated from the measurements shown in Sec. III A, which were affected by a limited time resolution.

The above discussion implies that amorphization is initiated at the borders of the molten pool with the surrounding crystalline matrix. This interpretation is in agreement with the images in Fig. 3, showing that the dark region corresponding to the liquid phase disappears via a shrinking process. As already pointed out in Sec. III A, the shrinking process is *not* driven by lateral heat flow but by heat flow toward the substrate, which has a r dependence due to the Gaussian intensity distribution of the pump pulse. The resulting lower local fluences at large r values lead to lower peak temperatures and shorter cooling times before the amorphous phase can be formed. We have studied this fluence dependence of the amorphization dynamics in detail by representing the temporal evolution of characteristic radial positions, marked in Fig. 4, $t=22$ ns. The result is shown in Fig. 5. The

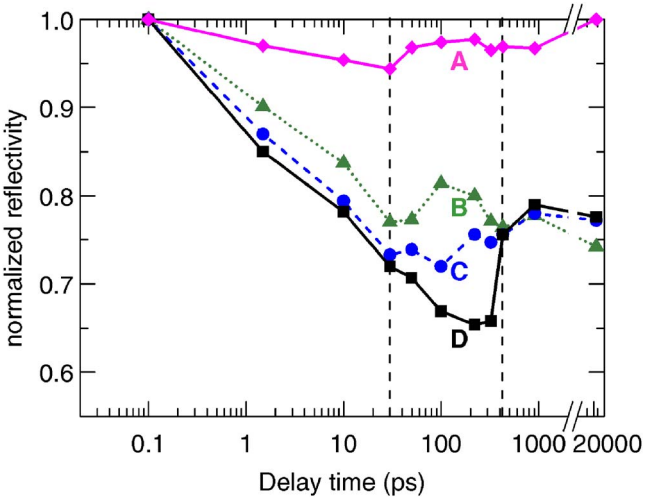

FIG. 5. (Color online) Temporal evolution of the normalized reflectivity (at 400 nm) at the characteristic radial positions A, B, C, and D marked in Fig. 4. The local fluences corresponding to the radial positions are $A=10.0$ mJ/cm^2, $B=36.6$ mJ/cm^2, $C=53.3$ mJ/cm^2, and $D=59.6$ mJ/cm^2. The vertical dashed lines mark the key delay times of 30 ps (thermalization time) and 430 ps (disappearance of the low-reflectivity phase).

temporal reflectivity evolution at radial position A (corresponding to a local fluence of 10.0 mJ/cm^2, where only heating occurs without permanent modification) is characterized by small and smooth changes. At $t=30$ ps the minimum value is reached, yielding a transient optical contrast of $\sim -5\%$. This relatively slow decay indicates that the transient optical changes are caused by the temperature dependence of the optical properties of the solid film.[22] This result is in contrast with the study on femtosecond excitation of amorphous $Ge_2Sb_2Te_5$ at similar fluences, in which a decay within less than 1 ps was observed.[23] Possible explanations for this difference may be the different laser parameters ($\lambda_{pump}=400$ nm, $\lambda_{probe}=800$ nm) and material phase (amorphous) used in Ref. 23. However, we do observe a fast component of the reflectivity recovery after the minimum (curve A in Fig. 5, between $t=30$ and $t=50$ ps), as reported in Ref. 23, and we also observe a slow component on a nanosecond scale.

At a local fluence sufficiently high to cause film melting and amorphization (radial position $B=36.6$ mJ/cm^2), the transient reflectivity decrease is much stronger but the minimum is reached at the same delay ($t=30$ ps) as for 10 mJ/cm^2 (position A). The further evolution of B is, however, very different. A slight increase at $t=100$ ps is followed by a corresponding decrease, remaining almost constant until the final value after irradiation. Although the origin of this oscillatory behavior at $t=100$ ps is not clear, we believe it is related to the fact that position B corresponds to a region where amorphization is not induced throughout the entire film thickness. In contrast, the evolution at position C, corresponding to a much higher fluence of 53.3 mJ/cm^2, shows a simpler behavior. Essentially, a reflectivity minimum is followed by a slight recovery at longer delays, yielding the reflectivity value of a completely amorphized film. The minimum reflectivity value that occurs at $t=100$ ps corresponds to the reflectivity value of the optically thick liquid phase, which is only somewhat below the one of the amorphous phase. As done in Sec. III A for a probe wavelength of 532 nm [cf. Fig. 2(b)], we have calculated also for 400 nm the expected reflectivity change upon transformation from the crystalline film into an amorphous film. While the evolution is found to be very similar (data not shown), a different value for the normalized minimum reflectivity is obtained. The calculated optical contrast at 400 nm for complete amorphization is -22%, which is in excellent agreement with the experimental value of $\sim -23\%$ (cf. Fig. 5, $R_{norm}=0.77$, $t=22\,000$ ps).

At the highest fluence studied (position $D=59.6$ mJ/cm^2), the reflectivity continues to decrease further after $t=30$ ps, reaching its minimum value as late as $t=220$ ps. Moreover the relative reflectivity decrease achieved in this case is $\sim -35\%$ ($R_{norm}\approx 0.65$). This value of R_{norm} is much smaller than the one obtained at the end of the amorphization process ($R_{norm}\approx 0.77$, $\sim -23\%$). This finding is consistent with the results reported by Kieu *et al.* upon picosecond laser irradiation,[15] who found reflectivity values of the liquid phase of $Ge_2Sb_2Te_5$ below the one of the amorphous phase. In comparison, the results reported in Ref. 9 indicated reflectivity values above that of the amorphous phase. However, those referred to a liquid phase induced at low fluences that did not lead to amorphization, which indicates incomplete melting. On the other hand, the reflectivity evolution at high fluences shown in Ref. 9 that did lead to amorphization shows indications of a transient reflectivity below the one of the amorphous phase. The much higher temporal resolution in our case makes it possible to identify unambiguously the presence of a transient liquid phase with anomalously low reflectivity at high fluences, close to the ablation threshold. The much later occurrence of the minimum at these high fluences (D), at a stage when the molten pool has begun to cool down rapidly, indicates that the anomalously low reflectivity value could be caused by extreme supercooling of the liquid phase. This interpretation is consistent with the fact that this phenomenon occurs in the center of the spot, where it is expected that the film is molten throughout its thickness. A direct contact of the melt with the substrate should favor efficient heat extraction, thus achieving large supercooling values. The fact that the low-reflectivity liquid phase vanishes abruptly and long after the laser pulse (between $t=325$ and 430 ps, cf. Figs. 3 and 5) excludes superheating of the liquid, as reported for Si (Ref. 24) and GeSb,[16] as a possible explanation for the low-reflectivity phase. It is also at $t=430$ ps that the reflectivity values of B, C, and D coincide (Fig. 5), indicating the end of the amorphization process over the entire spot diameter. The slight increase toward longer delay values is probably related to a combination of the temperature dependence of the optical properties of the hot solid and fluctuations of the probe beam intensity that lead to an error in the normalized reflectivity of $\sim \pm 0.02$ between different delays.

IV. CONCLUSIONS

The use of femtosecond laser pulses to induce amorphization in $Ge_2Sb_2Te_5$ films shows several advantages: The

virtual absence of heat diffusion during the femtosecond pulse results in sharp borders between the amorphized region and crystalline background and a more efficient energy deposition, implying lower fluence values. The higher supercooling achieved compared to nanosecond pulses leads to a complete amorphization throughout the entire film thickness, which should lead to a higher long-term stability due to the absence of crystalline seeds that may trigger spontaneous recrystallization. The higher supercooling also leads to much shorter transformation times than achievable with nanosecond pulses, yielding a minimum amorphization time of 100 ps at moderate fluences. At high fluences we have found evidence for the formation of a liquid phase with an anomalously low reflectivity immediately before the onset of amorphization. This points to a state of extreme supercooling of the liquid phase, favored by the high thermal conductivity of the Si substrate being responsible for the low reflectivity values.

ACKNOWLEDGMENTS

We are grateful to the authors of Ref. 18, in particular to Bong-Sub Lee, for helpful discussions concerning the analysis of the ellipsometry measurements and for providing their optical constants for comparison. This work has been partially supported by the EU projects CHEMAPH (IST-027561) and FLASH (MRTN-CT-2003-503641) and by the Spanish Ministry of Education and Science (Project TEC 2005-00074). D. P. acknowledges a grant of this Ministry and W. G. acknowledges the CSIC (I3P Programme contracts cofunded by the European Social Fund).

[1]S. R. Ovshinsky, Phys. Rev. Lett. **21**, 1450 (1968).
[2]http://en.wikipedia.org/wiki/Phase_change#Phase-change_data_storage.
[3]S. Lai, IEEE IEDM Tech. Dig., **2003**, 10.1.1.
[4]N. Yamada, E. Ohno, K. Nishiuchi, N. Akahira, and M. Takao, J. Appl. Phys. **69**, 2849 (1991).
[5]T. Ohta, N. Yamada, H. Yamamoto, T. Mitsuyu, T. Kozaki, J. Qiu, and K. Hirao, Mater. Res. Soc. Symp. Proc. **674**, V1.1.1 (2001); T. Ohta and N. Yamada, Proceedings of European Symposium on Phase Change and Ovonic Science, Schwägalb, Switzerland, (2001); T. Ohta and N. Yamada, http://www.epcos.org/papers/pdf_2001/Ohta.pdf.
[6]C. N. Afonso, J. Solis, F. Catalina, and C. Kalpouzos, Appl. Phys. Lett. **60**, 3123 (1992).
[7]M. C. Morilla, J. Solis, and C. N. Afonso, Jpn. J. Appl. Phys., Part 1 **36**, L1015 (1997).
[8]J. Siegel, C. N. Afonso, and J. Solis, Appl. Phys. Lett. **75**, 3102 (1999).
[9]J. Siegel, A. Schropp, J. Solis, C. N. Afonso, and M. Wuttig, Appl. Phys. Lett. **84**, 2250 (2004).
[10]T.-Y. Lee, K.-B. Kim, B.-K. Cheong, T. S. Lee, S. J. Park, K. S. Lee, W. M. Kim, and S. G. Kim, Appl. Phys. Lett. **80**, 3313 (2002).
[11]M. Wuttig, D. Lüsebrink, D. Wamwangi, W. Wełnic, M. Gilleßen, and R. Dronskowski, Nat. Mater. **6**, 122 (2007).
[12]K. Sokolowski-Tinten, J. Bialkowski, A. Cavalleri, D. von der Linde, A. Oparin, J. Meyer-ter-Vehn, and S. I. Anisimov, Phys. Rev. Lett. **81**, 224 (1998).
[13]J. Bonse, G. Bachelier, J. Siegel, and J. Solis, Phys. Rev. B **74**, 134106 (2006).
[14]C. Peng and M. Mansuripur, Appl. Opt. **43**, 4367 (2004).
[15]K. Kieu, K. Narumi, and M. Mansuripur, Appl. Opt. **45**, 7826 (2006).
[16]K. Sokolowski-Tinten, J. Solis, J. Bialkowski, J. Siegel, C. N. Afonso, and D. von der Linde, Phys. Rev. Lett. **81**, 3679 (1998).
[17]C. Wiemer, S. Ferrari, M. Fanciulli, G. Pavia, and L. Lutterotti, Thin Solid Films **450**, 134 (2004).
[18]B.-S. Lee, J. R. Abelson, S. G. Bishop, D. H. Kang, B. Cheong, and K. B. Kim, J. Appl. Phys. **97**, 093509 (2005).
[19]P. L. Liu, R. Yen, N. Bloembergen, and R. T. Hodgson, Appl. Phys. Lett. **34**, 864 (1979).
[20]M. O. Thompson, J. W. Mayer, A. G. Cullis, H. C. Webber, N. G. Chew, J. M. Poate, and D. C. Jacobson, Phys. Rev. Lett. **50**, 896 (1983).
[21]J. Siegel, J. Solis, and C. N. Afonso, J. Appl. Phys. **84**, 5531 (1998).
[22]N. Chaoui, J. Siegel, J. Solis, and C. N. Afonso, J. Appl. Phys. **89**, 3763 (2001).
[23]G. Zhang, F. Gan, S. Lysenko, and H. Liu, J. Appl. Phys. **101**, 033127 (2007).
[24]J. Boneberg, O. Yavas, B. Mierswa, and P. Leiderer, Phys. Status Solidi B **174**, 295 (1992).